Indium Tin Oxide-free Small Molecule Organic Solar Cells using Single-Walled Carbon Nanotube Electrodes

Clément Delacou[+][a], Il Jeon[+][a], Seungju Seo[a], Takafumi Nakagawa[a], Esko I. Kauppinen[b], Shigeo Maruyama[a,c]*, and Yutaka Matsuo[a,d] *

[a] Department of Mechanical Engineering, School of Engineering, The University of Tokyo, 7-3-1 Hongo, Bunkyo-ku, Tokyo, 113-8656, Japan.

[b] Department of Applied Physics, Aalto University School of Science, FI-00076 Aalto, Finland.

[c] National Institute of Advanced Industrial Science and Technology (AIST), 1-2-1 Namiki, Tsukuba, 305-8564, Japan.

[d] Hefei National Laboratory for Physical Sciences at the Microscale, University of Science and Technology of China, 96 Jinzhai Road, Hefei, Anhui 230026, China

[+] These authors contributed equally to this work.

* maruyama@photon.t.u-tokyo.ac.jp; matsuo@photon.t.u-tokyo.ac.jp

Abstract: We demonstrated single-walled carbon nanotubes (SWNTs) electrode-based small molecule organic solar cells (OSCs) using diketopyrrolopyrrole donor, DPP(TBFu)$_2$ as an electron donor with [6,6]-phenyl-C61-butyric acid methyl ester (PC$_{61}$BM) as an electron acceptor. SWNT films with 60% transmittance (at 550 nm) were dry-transferred onto glass substrates to replace conventional indium tin oxide (ITO) electrodes. In order to improve conductivity of the SWNT electrodes, MoO$_x$ thermal doping was applied followed by spin coating of poly(3,4-ethylenedioxythiophene):polystyrenesulfonate (PEDOT:PSS) to enhance doping and electrode blocking function. The indium-free devices showed a power conversion efficiency (PCE) of 1.00% while ITO-based devices showed a PCE of 3.79%.

Introduction

The Low-cost and eco-friendly nature of organic solar cells (OSCs) has drawn a great deal of attention as the next-generation renewable energy. Owing to the recent development of low band-gap polymers, power conversion efficiency (PCEs) of OSCs now reach more than 10% for a non-tandem device.[1–3] In OSCs, expensive indium tin oxide (ITO) is used as the transparent conductive electrode. However, indium in ITO is rare and the ITO has a brittle property, which limits the flexible application of OSCs.[4] Single-walled carbon nanotubes (SWNTs), on the other hand, have excellent electrical, optical, and mechanical properties. They are composed only of carbon, so the raw material is technically earth-abundant. In addition, aerosol-synthesised SWNT films used in this work are easy to transfer onto other substrates.[5] Therefore, SWNT film is a perfect candidate for ITO replacement. We have already reported SWNT-based OSCs using low band-gap polymers as the electron donor, and produced a high PCE similar to that of the ITO reference devices.[6]

In this work, we used small molecules as the electron donor to test their viability in SWNT-based OSCs. Solution-processed small molecule bulk heterojunction (BHJ) devices demonstrate similar efficiencies to their

polymer-based counterparts.[7,8] Low molecular weight small molecule donors have high absorption coefficient, fast charge transport, and enhanced miscibility with the fullerene acceptors.[9–11] In fact, the advantages of these small molecule semiconductors over low band-gap polymers are that they have low batch-to-batch variation, easy to modify chemically, and show excellent miscibility with fullerenes. Different types of small molecule donors for BHJ OSCs were reported in great number:[9] One of the exemplary small molecule donors is diketopyrrolopyrrole (DPP) with a high field-effect mobility due to good π–π stacking interactions involving fused aromatic rings in a planar conjugated polymer.[12–20] DPP and fullerene derivative combinations produced high PCEs.[21–23] Therefore, we fabricated small molecule OSCs using a combination of the DPP-based small molecule electron donor, DPP(TBFu)$_2$ and PC$_{61}$BM in a BHJ.

Results and Discussion

Device Performance and Comparison

OSCs were fabricated using a BHJ of DPP(TBFu)$_2$ and PC$_{61}$BM on SWNT films using thermal MoO$_x$ doping (Fig. 1). Anaerobic thermal doping of MoO$_3$ next to SWNTs was found to be a stable and effective doping method.[6,24] SWNT films were prepared by direct and dry deposition of SWNTs grown by the floating catalyst, *i.e.,* aerosol chemical vapor deposition technique and deposited on a nitrocellulose membrane.[25] For this study, we produced SWNT films of 60% transparency at 550 nm and transferred them onto bare glass substrates. 15-nm-thick MoO$_3$ was thermally deposited on the SWNT films and they were annealed at 300 °C for 2 hours under N$_2$. The color change of MoO$_3$ to green meant the formation of MoO$_x$ where x is between 2 and 3. This is an indicative of a successful *p*-doping. To further enhance the hole diffusion to the SWNT electrode and improve morphology, PEDOT:PSS was spin-coated above MoO$_x$. The active layers were prepared from a 20 mg mL^{-1} solution with a donor to acceptor ratio of 3:2 in CHCl$_3$ which is a typical solvent for DPP.[26] The spin-coating speed and annealing temperature, which define, respectively the thickness and crystallization of the organic bulk-heterojunction active layer, were optimized. Then LiF and Al were deposited by thermal evaporation to complete the device fabrication (see device fabrication for more details).
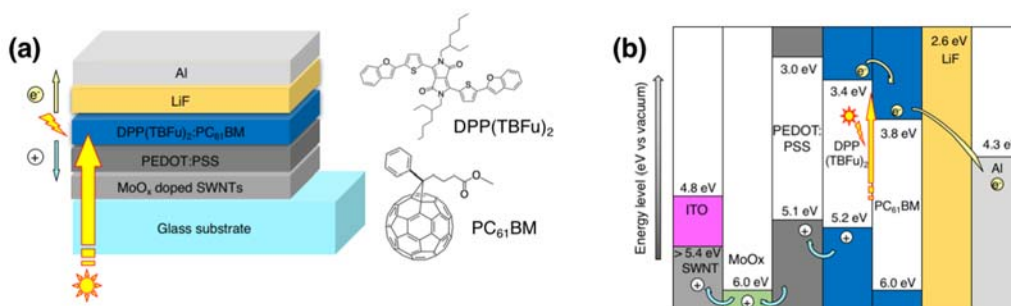

Figure 1: (a) Schematic of the device architecture and molecular structures of DPP(TBFu)$_2$ and PC$_{61}$BM. (b) Energy band alignment diagram of the SWNT-based small molecule OSC.

The photovoltaic result in Table 1 shows that the ITO reference devices produced a PCE of around 3.79%. Because we did not encapsulate the devices, this value can be regarded a typical PCE for a DPP-based OSC. The SWNT-based devices produced a PCE of 1.00 %. Interestingly, the SWNT-based devices produced substantially low short-circuit current density (J_{SC}) of 3.16 mA cm^{-2} than that of the ITO references (9.38 mA cm^{-2}). Open-circuit voltage (V_{OC}) and fill factor (FF), on the other hand, were similar or slightly lowered for the SWNT-based devices to the reference devices. V_{OC} indicates that the coating coverage of the active layer, so we can deduce that the SWNT-based OSCs had good coverage. Low FF value points to the fact that either the conductivity of the SWNT electrode or the recombination of the charges within the system is the reason. FF is influenced by series resistance (R_S) and shunt resistance (R_{SH}). Similar R_S values indicate that the SWNT films had good conductivity and the doping was successful. However, the low value of R_{SH} for the SWNT-based devices means that there was significant charge recombination, which is suspected to be the main reason for the lower FF.

Table 1: Photovoltaic parameters of the devices measured under standard one-sun conditions (AM 1.5G, 100 mW cm^{-2}).

| Entry	Anode	V_{OC} (V)	J_{SC} (mA/cm^2)	FF	R_S (Ω cm^2)	R_{SH} (Ω cm^2)	PCE (%)
1	SWNTs	0.80	3.16	0.40	40.2	2.16×10^4	1.00
2	ITO	0.86	9.38	0.49	22.4	1.67×10^6	3.79

Figure 2 shows the current density and voltage (J–V) curve of the devices, and we can observe that both of the devices have a similar horizontal gradient for the J–V curves which means that they have similar R_S. Both of the J–V curves show a similar rectangular shape, due to similar FF.
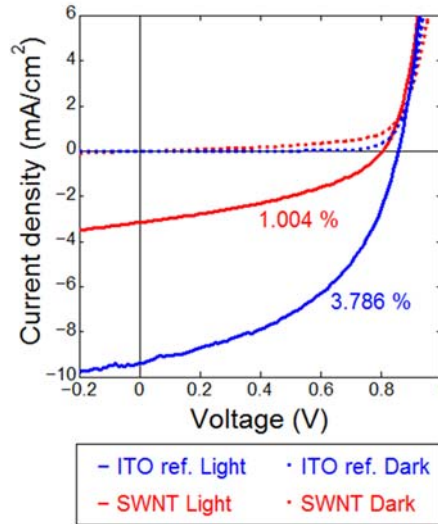
Figure 2. J−V curves of the devices using the SWNT electrode (solid red) and ITO (solid blue) under light; and SWNT electrode (dotted red) and ITO (dotted blue) under dark.

Morphological Analysis

To investigate the morphology of the devices, we used cross-sectional scanning electron microscopy (SEM) (Figure 3). We noticed that active layer spin coated on ITO was more uniform than that on an SWNT electrode. Also, the thickness of the active layer was thicker for the ITO devices. We suspect that this is because the rougher surface of SWNTs leads to less homogeneous active film and some of the active solution gets absorbed into the nanotube network due to the small size of small molecules.
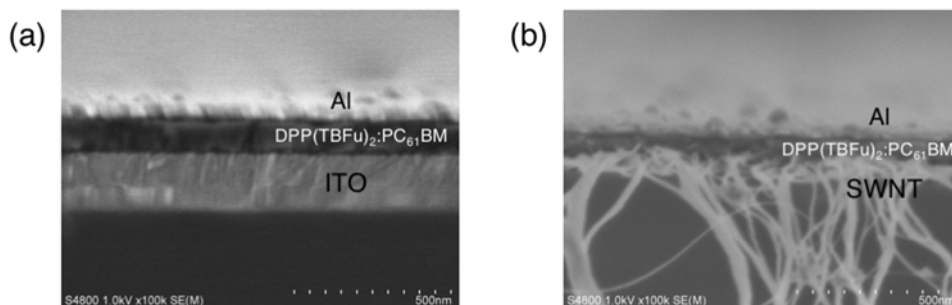
Figure 3. Cross-section SEM pictures of a) ITO-based and b) SWNT-based devices (100k magnification).

To understand the interface between the active layer and the electrode, we performed atomic force microscopy (AFM) and observed the roughness of active layers, ITO and an SWNT film (Figure 4). The active layers were on PEDOT:PSS-applied ITO glass and a PEDOT:PSS-capped MoO_x-deposited SWNT film, each. According to Figure 4 a and b, ITO had much smoother surface than the SWNT film as ITO had a root mean square roughness (RMS) of 3.2 nm while the SWNT film had an RMS of 10.8 nm. These led to the difference in the roughness of the active layers. The spin-coated active layer on ITO/PEDOT:PSS had an RMS of 1.86 nm, while the active layer on SWNT/MoO_x/PEDOT:PSS possessed a RMS of 9.18 nm (Figure 4c and d). Figure 4d shows that the surface roughness resembled the SWNTs underneath the active layer. We surmise that the small molecules were percolated into the SWNT network. In other words, the small molecule-based active layer should not be spin-coated on a rough and porous surface, such as SWNTs.
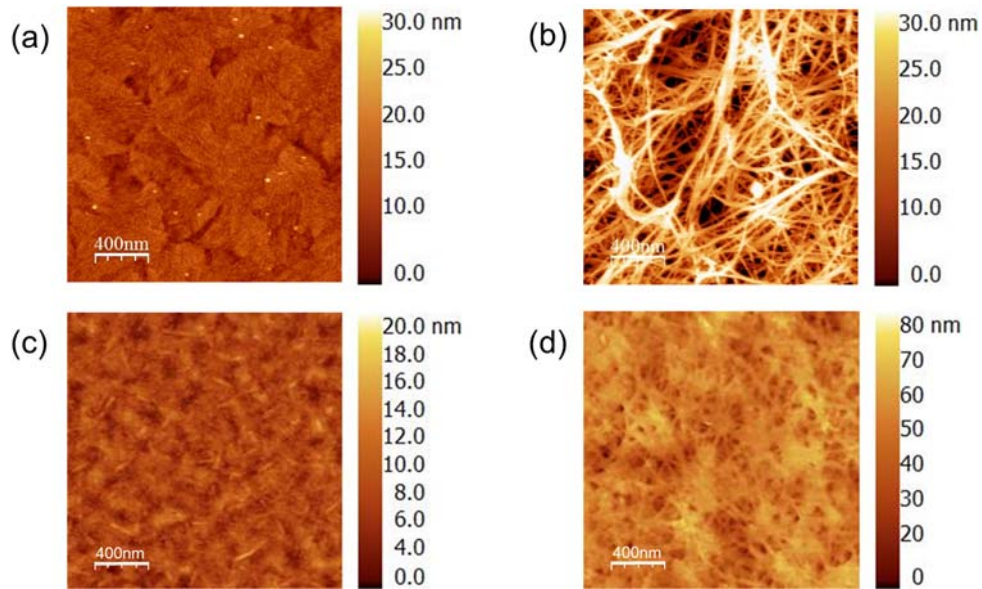
Figure 4. AFM pictures of a) glass/SWNT, b) glass/ITO, c) glass/ITO/PEDOT:PSS/ DPP:PC$_{61}$BM, and d) glass/SWNT/MoOx/PEDOT:PSS/ DPP: PC$_{61}$BM.

Optical Analysis

We measured UV-vis transmittance of various substrates (Figure 5). This is important, because optical transparency has a direct impact on photocurrent, as represented by J_{SC}. Figure 5a shows the transmittance data of the SWNT film (60% transmittance at 550 nm) on glass and ITO on glass. It is clear that the SWNT film has much lower transparency than ITO. However, upon thermal doping of MoO$_x$, the transparency of the SWNT film improved. This could be the effect of doping, the antireflective effect of MoO$_x$ layer, or both. Figure 5b shows UV-vis transmittance data of the electrodes with the active material. Here, we can observe the difference between the two data; this accounts for the lower J_{SC} of the SWNT-based OSCs. However, because the difference in transmittance is less than half, we attribute the poor morphology of the active layer to be responsible for the low J_{SC}, which is approximately three times lower for the SWNT-based OSCs.
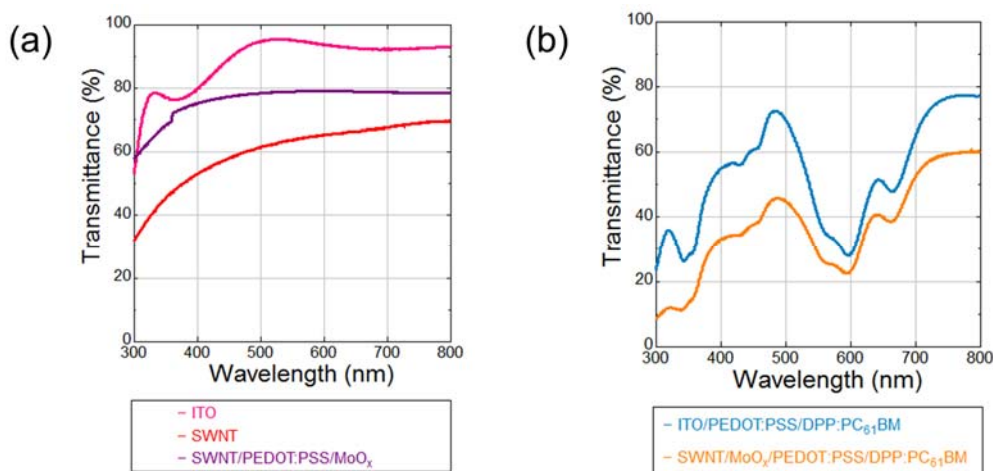
Figure 5. UV-vis transmittance data of a) electrodes: glass/ITO (pink), glass/SWNT film (red), and glass/SWNT/MoO$_x$/PEDOT:PSS (purple); and b) electrodes with the active material: ITO/PEDOT:PSS/DPP:PC$_{61}$BM (sky blue) and SWNT/MoO$_x$/PEDOT:PSS/ DPP: PC$_{61}$BM (orange).

Conclusion

SWNT aerosol film was thermally *p*-doped by MoO$_x$ and applied as the anode in small molecule OSCs in which a mixture of DPP(TBFu)$_2$ and PC$_{61}$BM was employed. The SWNT-based OSCs gave a PCE of 1.00%, while the ITO control-devices gave 3.79%. The V_{OC} and FF were sufficiently high for the SWNT-based OSCs, which indicated full coverage of the active layer and a successful doping, respectively. Nevertheless, substantially low J_{SC} was due to the poor morphology induced by rough CNT network and the lower transparency of the SWNT films. We conclude that the application of small molecule-based bulk heterojunction may be difficult on SWNT electrodes. We underline that the possibility of using small molecule active layer over an SWNT electrode with MoO$_x$ doping and PEDOT:PSS capping is low.

Experimental Section

Aerosol SWNT preparation

SWNTs were synthesized by an aerosol (floating catalyst) CVD method based on ferrocene vapor decomposition in a CO atmosphere. The catalyst precursor was vaporized by passing ambient temperature CO through a cartridge filled with ferrocene powder. The flow containing ferrocene vapor was then introduced into the high-temperature zone of a ceramic tube reactor through a water-cooled probe and mixed with additional CO. To obtain stable growth of SWNTs, a controlled amount of CO$_2$ was added together with the carbon source (CO). SWNTs were directly collected downstream of the reactor by filtering the flow through a nitrocellulose or silver membrane filter (Millipore Corp., USA; HAWP, 0.45 μm pore diameter).

Organic semiconductors

3,6-Bis[5-(benzofuran-2-yl)thiophen-2-yl]-2,5-bis(2-ethylhexyl)pyrrolo[3,4-c]pyrrole-1,4dione (DPP(TBFu)$_2$) was purchased from Lumtec and further purified by column chromatography on silica gel (Wakogel® 60N) by using chloroform as the eluent.

Device Fabrication

A device was fabricated with the following architecture: Glass/SWNT/MoO$_x$/poly(3,4-ethylenedioxythiophene) (PEDOT):polystyrenesulfonate (PSS)/DPP(TBFu)$_2$:PC$_{61}$BM/LiF/Al. First, bare glass substrates were sonicated in acetone for 20 min followed by two additional 20 min sonication cycles in isopropanol. Next, the substrates were dried under a stream of nitrogen and then subjected to 30 min UV/O$_3$ treatment. SWNT films were transferred onto the cleaned glass substrates by laminating from the top. A drop of ethanol was used to ensure firm adhesion of SWNTs. Then the substrates were transferred to a nitrogen filled glove box for further fabrication. MoO$_3$ film was deposited under vacuum via a thermal evaporator. 15 nm MoO$_3$ was deposited with the average rate of 0.2 Å/s. For MoO$_x$ doping, it was annealed at 300 °C for 2 h in N$_2$. PEDOT:PSS (Clevios AI4083) was spin-coated onto the clean ITO substrates at a rate of 4500 rpm for 45 s in air. Drying of the PEDOT:PSS films was first achieved in air at 120 °C for 10 min and then in a nitrogen-filled glove box at 130 °C for an additional 5 min. The optimized donor/acceptor ratio (w/w) for DPP(TBFu)$_2$:PC$_{61}$BM was 3:2 in a total concentration of 20 mg/mL in CHCl$_3$, this organic solution was stirred at 50 °C for 3 hours. Active layers were then deposited by spin-coating at a rate of 4500 rpm for 60 s (optimized spin-coating for devices using ITO anode). The active-layer thickness was approximately 90 nm, as measured by using a step profiler and confirmed on SEM pictures. For the active layers after spin-coating, TA was performed by placing the samples on a hot plate at a temperature of 90 °C under nitrogen (optimized annealing temperature for devices using ITO anode). Following the annealing process, the substrates were placed in an evaporator chamber, in which a 0.8 nm layer of LiF was first deposited followed by a 100 nm thick layer of Al. The pressure of the evaporation chamber never exceeded 5 x 10^{-4} Pa during deposition. For making reference devices, patterned ITO on glass substrates (155 nm, 9 W/sq.) were used following previously described steps for the following architecture: Glass/ITO/PEDOT:PSS/DPP(TBFu)$_2$:PC$_{61}$BM/LiF/Al.

Device Characterization

Current–voltage (J–V) characteristics were measured by using a software-controlled source meter (Keithley 2400) under dark conditions and one sun AM 1.5G simulated sunlight irradiation (100 mW/cm^2) by using a solar simulator (EMS-35AAA, Ushio Spax Inc.), which was calibrated by using a silicon diode (BS-520BK, Bunkokeiki).

Keywords: carbon nanotubes · small molecules · organic solar cells · MoO$_x$ doping · indium-free solar cells

References

1.	J. Zhao, Y. Li, G. Yang, K. Jiang, H. Lin, H. Ade, W. Ma, and H. Yan, *Nat. Energy*, **1**, 15027 (2016).

2.	J. Huang , J. H. Carpenter , C.-Z. Li, J.-S. Yu , H. Ade, and A. K.-Y. Jen, *Adv. Mater.*, **28**, 967 (2016).

3.	J.-D. Chen, C. Cui, Y.-Q. Li, L. Zhou, Q.-D. Ou, C. Li, Y. Li, and J.-X. Tang, *Adv. Mater.*, **27**, 1035 (2014).

4.	I. Jeon, T. Chiba, C. Delacou, Y. Guo, A. Kaskela, O. Reynaud, E. I. Kauppinen, S. Maruyama, and Y. Matsuo, *Nano Lett.*, **15**, 6665 (2015).

5.	A. Kaskela, A. G. Nasibulin, M. Y. Timmermans, B. Aitchison, A. Papadimitratos, Y. Tian, Z. Zhu, H. Jiang, D. P. Brown, A. Zakhidov, and E. I. Kauppinen, *Nano Lett.*, **10**, 4349 (2010).

6.	I. Jeon, K. Cui, T. Chiba, A. Anisimov, A. G. Nasibulin, E. I. K.auppinen, S. Maruyama, and Y. Matsuo, *J. Am. Chem. Soc.*, **137**, 7982 (2015).

7.	A. K. K. Kyaw, D. H. Wang, V. Gupta, J. Zhang, S. Chand, G. C. Bazan, and A. J. Heeger, *Adv. Mater.*, **25**, 2397 (2013).

8.	Y. Liu, C.-C. Chen, Z. Hong, J. Gao, Y. M. Yang, H. Zhou, L. Dou, G. Li, and Y. Yang, *Sci. Rep.*, **3**, 3356 (2013).

9.	J. Roncali, P. Leriche, and P. Blanchard, *Adv. Mater.*, **26**, 3821 (2014).

10.	B. Walker, C. Kim, and T.-Q. Nguyen, *Chem. Mater.*, **23**, 470 (2011).

11.	H. Sirringhaus, M. Bird, and N. Zhao, *Adv. Mater.*, **22**, 3893 (2010).

12.	Z. Li, Y. Zhang, S.-W. Tsang, X. Du, J. Zhou, Y. Tao, and J. Ding, *J. Phys. Chem. C*, **115**, 18002 (2011).

13.	T.L. Nelson, T.M. Young, J. Liu, S.P. Mishra, J.A. Belot, C.L. Balliet, A.E. Javier, T. Kowalewski, and R.D. McCullough, *Adv. Mater.*, **22**, 4617 (2010).

14.	T.K. An, I. Kang, H. Yun, H. Cha, J. Hwang, S. Park, J. Kim, Y.J. Kim, D.S. Chung, S.-K. Kwon, Y.-H. Kim, and C.E. Park, *Adv. Mater.*, **25**, 7003 (2013).

15. P. Sonar, J.-M. Zhuo, L.-H. Zhao, K.-M. Lim, J. Chen, A.J. Rondinone, S.P. Singh, L.-L. Chua, P.K.H. Ho, and A. Dodabalapur, *J. Mater. Chem.*, **22**, 17284 (2012).

16. S. Cho, J. Lee, M. Tong, J.H. Seo, and C. Yang, *Adv. Funct. Mater.*, **21**, 1910 (2011).

17. Y. Li, S.P. Singh, and P. Sonar, *Adv. Mater.*, **22**, 4862 (2010).

18. J.S. Ha, K.H. Kim, and D.H. Choi, *J. Am. Chem. Soc.*, **133**, 10364 (2011).

19. A.J. Kronemeijer, E. Gili, M. Shahid, J. Rivnay, A. Salleo, M. Heeney, and H. Sirringhaus, *Adv. Mater.*, **24**, 1558 (2012).

20. A.B. Tamayo, X.-D. Dang, B. Walker, J. Seo, T. Kent, and T.-Q. Nguyen, *Appl. Phys. Lett.*, **94**, 103301 (2009).

21. A.B. Tamayo, M. Tantiwiwat, B. Walker, and T.-Q. Nguyen, *J. Phys. Chem. C*, **112**, 15543 (2008).

22. C. Kim, J. Liu, J. Lin, A.B. Tamayo, B. Walker, G. Wu, and T.-Q. Nguyen, *Chem. Mater.*, **24**, 1699 (2012).

23. I. Jeon, C. Delacou, T. Nakagawa, and Y. Matsuo, *Chem. - An Asian J.*, **11**, 1268 (2016).

24. S.L. Hellstrom, M. Vosgueritchian, R.M. Stoltenberg, I. Irfan, M. Hammock, Y.B. Wang, C. Jia, X. Guo, Y. Gao, and Z. Bao, *Nano Lett.*, **12**, 3574 (2012).

25. A.G. Nasibulin, A. Ollikainen, A.S. Anisimov, D.P. Brown, P. V. Pikhitsa, S. Holopainen, J.S. Penttilä, P. Helistö, J. Ruokolainen, M. Choi, and E.I. Kauppinen, *Chem. Eng. J.*, **136**, 409 (2008).

26. A. Viterisi, F. Gispert-Guirado, J. W. Ryan, and E. Palomares, *J. Mater. Chem.*, **22**, 15175 (2012).